



## Advanced top-attack trajectory guidance law with impact angle

Original  
Article

Abdallah Mamdouh Abu El-Wafa, Mohammed Abozied Hassan, Yehia Zakria Elhalwagy and Hossam M. Hendy

Department of Guidance and Control, Military Technical College, Cairo, Egypt

### Keywords:

Anti-tank missile, impact angle constraints, top-attack

### Corresponding Author:

Abdallah Mamdouh Abu El-Wafa, Military Technical College, Tel: 01558668031, Email: abdallah.mamdouh.54@gmail.com

### Abstract

Recently, there has been a renewed interest in the development of battle tanks armoring, which made old generations of anti-tank missiles are no longer able to counteract modern tanks by hitting armor in the front or the side sections of the tank. Recent developments directed toward designing the antitank missiles to hit the tank from the upper ceiling which is considered one of the weakest points in the tank armor. The new generations of anti-tank missiles are developed with the ability to hit tanks from its upper section (top-attack). So, the current article focuses on developing the antitank missile guidance law to generate a top-attack trajectory considering (impact angle, missile maneuverability, miss distance) constraints. The accuracy of the generated trajectory is evaluated through two main parameters, impact angle and miss distance, a polynomial function based trajectory is proposed. Further extended analysis is carried out for evaluating missile motion parameters via a 6-DOF model. The proposed algorithm is simulated utilizing Matlab/Simulink with different scenarios.

## I. INTRODUCTION

Anti-Tank Guided Missiles (ATGM) are an essential and important element of arming most armies around the world, as they are one of the practical and relatively inexpensive means to defeat enemy armored forces in both defensive or offensive operations or even in special forces operations<sup>[1]</sup>. Anti-armor missiles could be often divided into 3 Generations or more, as the command to line of sight guidance law is the main concept for both first and second-generation ATGMs, the 1st and 2nd generation of ATGMs are flawed by the necessity to be a man in the loop during the flight period of the missile until it collides with the target, and the guidance trajectory enables missiles to hit the armor from the front and the sides where the armor is thicker and more resilient to missiles' strikes. Therefore, the need for new developments for anti-tank guided missiles has arisen to enable them to attack tanks at the weakest possible point of the armor "the upper ceiling of the tank" with a certain impact angle. To overcome these limitations, the 3rd generation of ATGMs was developed, which is always known by two main features "Fire & Forget" and "Top-Attack" capabilities<sup>[2]</sup> and<sup>[3]</sup>. Impact angle constrained laws of guidance have become essential for 3rd generations ATGMs and modern warfare in general. The drive to achieve a certain terminal impact angle often stems from the need to increase the lethality of the warhead in case of direct strikes even on the hostile tanks' armors, which are usually designed with specific inclinations. Also, a good

impact angle constrained guidance provides the stealthiness of the missile, while the missile can evade the active/passive protection systems that modern tanks are equipped with<sup>[4]</sup>. For each engagement scenario, a minimum miss distance is required to be achieved as well as a suitable terminal impact angle to ensure more damage effect<sup>[5]</sup>. For all of these reasons, the impact angle constrained guidance problems have occupied the attention of many researchers in the field of the guided weapons and missiles<sup>[6]</sup>. Through this paper a 3rd-degree polynomial based guidance law with impact angle constrained is introduced for shaping a pre-designed top-attack trajectory for ATGM, which is characterized by passive guidance, limiting the possibility of disturbances in its flight, and the ability to lock on a target before launch what is known as "LOBL" in "Fire-and-Forget" mode or lock on a target after launch in what is known as "LOAL"<sup>[2]</sup>. Usually, 3rd generation ATGMs are equipped with IIR/CCD seekers which provide a live view of the battlefield, identify the target, send a real-time target seen to the monitor on the launching position via a wireless data-link or a fiber-optic cable during flight. Also, correction of the trajectory and target-selection during the flight are optional for the shooter by sending corrective signals to the missile via two-way data-link, till reaching a certain point from which the guidance is switched to self-guidance<sup>[7]</sup>. For this flight mode with a "man in the control loop", the initial approximate location of the target is sufficient to determine the trajectory to enable the shooter to attack targets that might be hiding behind buildings or

natural terrain from the upper ceiling, that feature gives an important tactical advantage in the battlefield.

The 3rd generation ATGM can attack a target directly along the line of sight as well as the upper ceiling, but the missile isn't controlled from the launcher like the older generation (self-guidance). The decision to attack a target from the upper ceiling or directly along the line of sight is constrained by the target range and the missile maneuverability. In case of a direct attack along the line of sight "usually for short ranges", the missile is guided to the target through a programmed semi-straight path, as the missile makes a limited maneuver in the elevation plane due to the missile's preflight attitudes "launcher attitudes" and the target's range, while in case of attacking a target from the upper ceiling "usually for long ranges", the missile is guided through a programmed curved path. In "Fire-and-Forget" or "LOBL" mode, the shaping of the trajectory is constrained by the seeker capability as the seeker's look angle mustn't exceed its maximum permissible value "in case of gimballed seeker" or the seeker's field of view "in case of stabilized seeker" for the entire period of the flight[8]. It must be emphasized that automatic control of the ATGM using a polynomial function affects the reduction of human interference in the guidance process of the 3rd generation ATGM from the launching moment until the destruction of the target. The paper introduces algorithms that allow the above requirements to be met.

In section 2 the guidance algorithm is introduced. Section 3 describes the control criteria. Section 4 describes the ATGM equations of motion. Time-domain 6-DOF simulation results for some case studies in section 5. The

conclusion of the work is presented in section 6.

## I. THE GUIDANCE ALGORITHM OF ATGM

### A. The concept of the guidance algorithm

The implementation of the algorithm is to control the flight in such a way that it follows the specified flight path. In that case, follow the curve of a polynomial. The most popular control method includes various types of error control. This method consists of introducing control forces  $Q$  which depend on the current deviation of the performed trajectory from the designed one<sup>[9]</sup>.

To determine the error, it is necessary to provide feedback informing the control system with the performed flight parameters as a result of the control. The methods for obtaining this information differ in many solutions, but two main groups of solutions can be divided into.

Autonomous ones which independently determine their location, whether based on sensors like Inertial Measurement Unit (IMU) that track the flight parameters (such as acceleration, angular velocity, and their integrations) or applying other methods for navigation. Non-Autonomous ones, in which Observation and Tracking Devices are used to obtain the required information (self-guidance – the 2nd stage of the flight on LOAL mode), i.e. "commands from launcher" (remote self-guidance).

Observation and Tracking Devices (OTD) can also illuminate a target for the missile (as the illuminated target is considered as the final point of the curve)[10]. Considerations regarding the algorithm include three possibilities of attacking armored objects.

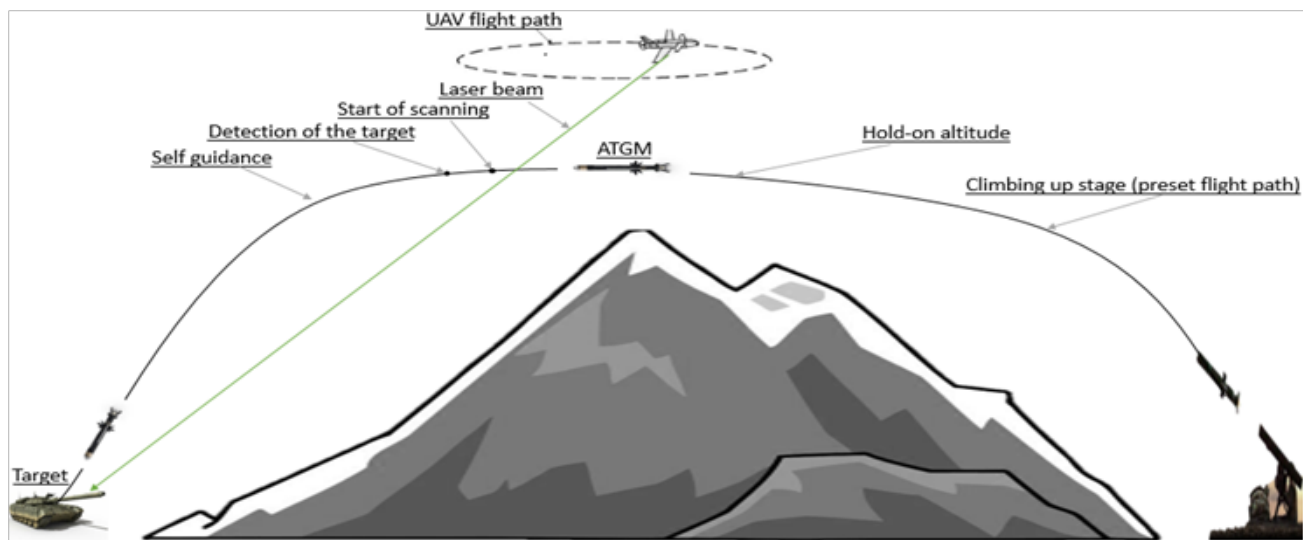


Fig. 1: General view of the guidance of the ATGM on LOAL mode (using a laser beam emitted from UAV)

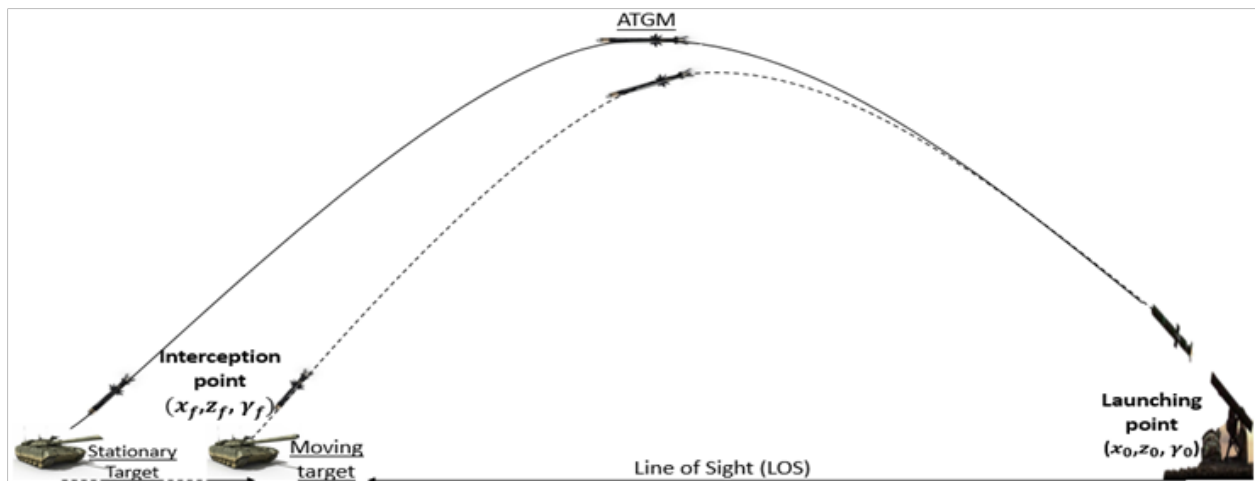


Fig. 2: General view of the guidance of the ATGM on LOBL mode (initial data is obtained using OTD of the launcher)

As shown in Figure 1, slowly moving hiding targets at relatively large distances require the range of the missiles whose flight is divided into the programmed flight, tracking, and autonomous guidance.

In Figure 2, Target at a relatively large distance but in the immediate range of vision of the launcher's OTD, in which just two points (launching point & interception point) are sufficient for shaping the trajectory.

In all cases, the algorithm assumes attack on the upper surface of the armored body<sup>[8]</sup>.

flying vehicle has an Axisymmetric configuration with "+" configuration rear fins, which are responsible for controlling the missile's manoeuvrability.

B- Numerical calculations of the algorithm in the vertical plane:

The flight path of the ATGM is described using the

third-degree polynomial<sup>[10]</sup>. Correct selection of (a, b, c, and d) coefficients with successive powers allows the variable x to be formed correct flight curve, based on the input initial and final points and their related slopes. The missile's flight path is divided into successive stages with beginning and ending at certain points.

$$z = ax^3 + bx^2 + cx + d \quad (1)$$

$$\gamma = \tan^{-1}(3ax^2 + 2bx + c) \quad (2)$$

$$(x_0, z_0, \gamma_0) \quad . \quad (x_f, z_f, \gamma_f)$$

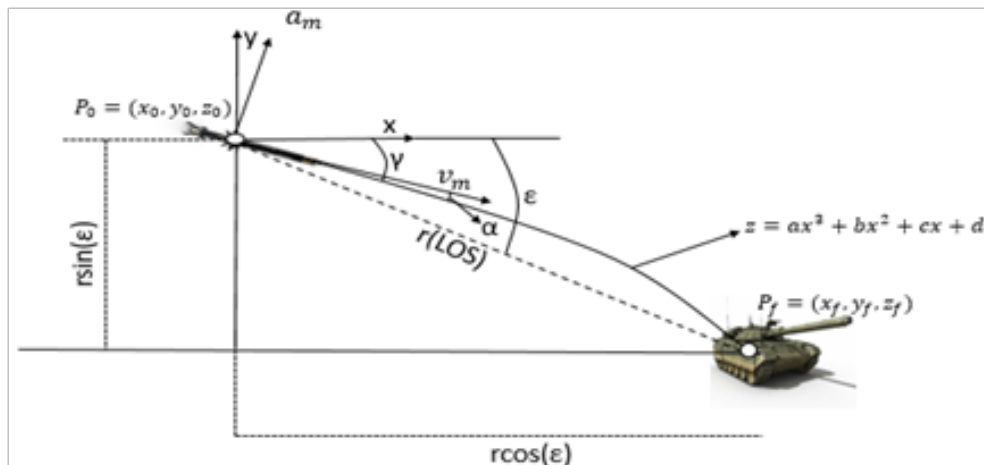


Fig. 3: A missile attacks the target from the diving point

Planar engagement scenario between the missile and the target is demonstrated as shown in Figure 3,  $v_m$  and  $v_t$  are the missile velocity and target velocity respectively, and  $a_m$  and  $a_t$  represent their normal accelerations, respectively. The initial points of the curve  $x_0$  and  $z_0$  and the flight path angle  $\gamma_0$  are obtained using the missile navigation system, while the missile's seeker provides the Line-of-Sight angle ( $\varepsilon$ ) and closing range ( $r$ ). The relation between the Cartesian and Polar coordinates is as in equation (3) and (4):

$$x_f - x_0 = r \sin(\varepsilon) \quad (3)$$

$$z_f - z_0 = r \cos(\varepsilon) \quad (4)$$

For each scenario, the flight path angle at the interception point is programmed to a certain value to achieve the demanded impact angle.

From the set of four equations that contain four unknown values which are variable coefficients

$$ax_0^3 + bx_0^2 + cx_0 + d = z_0 \quad (5)$$

$$3ax_0^2 + 2bx_0 + c = \tan(\gamma_0) \quad (6)$$

$$ax_f^3 + bx_f^2 + cx_f + d = z_f \quad (7)$$

$$3ax_f^2 + 2bx_f + c = \tan(\gamma_f) \quad (8)$$

We get the following system (matrix) to be solved

$$\begin{bmatrix} a \\ b \\ c \\ d \end{bmatrix} = \begin{bmatrix} x_0^3 & x_0^2 & x_0 & 1 \\ 3x_0^2 & 2x_0 & 1 & 0 \\ x_f^3 & x_f^2 & x_f & 1 \\ 3x_f^2 & 2x_f & 1 & 0 \end{bmatrix}^{-1} \begin{bmatrix} z_0 \\ \tan(\gamma_0) \\ z_f \\ \tan(\gamma_f) \end{bmatrix} \quad (9)$$

During the entire flight, when dealing with a moving target, the coefficients are sequentially calculated (each successive coefficient comprises the previous ones).

$$a = \frac{-2z_f + 2z_0 - (x_0 - x_f)(\tan(\gamma_f) + \tan(\gamma_0))}{(x_f - x_0)^3} \quad (10)$$

$$b = \frac{\tan(\gamma_0) - \tan(\gamma_f) - (3x_0^2 - 3x_f^2)}{2x_0 - 2x_f} \quad (11)$$

$$c = \tan(\gamma_f) - 3ax_f^2 - 2bx_f \quad (12)$$

$$d = z_f - ax_f^3 - bx_f^2 - cx_f \quad (13)$$

Missile interception with moving target with impact angle constraints<sup>[11]</sup>.

The flight path angle at the interception point is evaluated like:

$$\dot{\gamma}_m = \frac{a_m}{v_m} \quad \text{and} \quad \dot{\gamma}_t = \frac{a_t}{v_t} \quad (14)$$

Where,

$$\varepsilon_t = \gamma_t - \varepsilon \quad \text{and} \quad \varepsilon_m = \gamma_m - \varepsilon \quad (15)$$

$$\varepsilon_{imp} = \gamma_{tf} - \gamma_{mf} \quad (16)$$

$\varepsilon_{imp}$  is the desired impact angle, which is the angle between the missile velocity vector and the target at the moment of interception,  $\gamma_{mf}$  and  $\gamma_{tf}$  are the flight path angles of the missile and target respectively. When the missile and target on a collision stage, the Line-of-Sight angle is defined by  $\varepsilon_f$  and the relation between the missile and target

$$v_m \sin(\varepsilon_{mf}) = v_t \sin(\varepsilon_{tf}) \quad (17)$$

Where,

$$\varepsilon_{mf} = \gamma_{mf} - \varepsilon_f \quad \text{and} \quad \varepsilon_{tf} = \gamma_{tf} - \varepsilon_f \quad (18)$$

We have  $(r\varepsilon) = 0$ , at the interception point.

$$\varepsilon_f = \gamma_{tf} - \tan^{-1}\left(\frac{\sin(\varepsilon_{imp})}{\cos(\varepsilon_{imp}) - \eta}\right)$$

$$\text{Where, } \eta = \frac{v_t}{v_m} \quad \text{that } v_t < v_m \quad (19)$$

From (16), and (19)

$$\gamma_f = \gamma_{mf} = \tan^{-1}\left(\frac{\sin(\varepsilon_{imp})}{\cos(\varepsilon_{imp}) - \eta}\right) \quad (20)$$

So equation (9) is modified to be:

$$\begin{bmatrix} a \\ b \\ c \\ d \end{bmatrix} = \begin{bmatrix} x_0^3 & x_0^2 & x_0 & 1 \\ 3x_0^2 & 2x_0 & 1 & 0 \\ x_f^3 & x_f^2 & x_f & 1 \\ 3x_f^2 & 2x_f & 1 & 0 \end{bmatrix}^{-1} \begin{bmatrix} z_0 \\ \tan(\gamma_0) \\ z_f \\ \tan(\tan^{-1}(\frac{\sin(\varepsilon_{imp})}{\cos(\varepsilon_{imp})-\eta})) \end{bmatrix} \quad (21)$$

For stationary target, it's obvious that  $\gamma_{mf} = \varepsilon_{imp}$ .

## II. THE CONTROL ALGORITHM

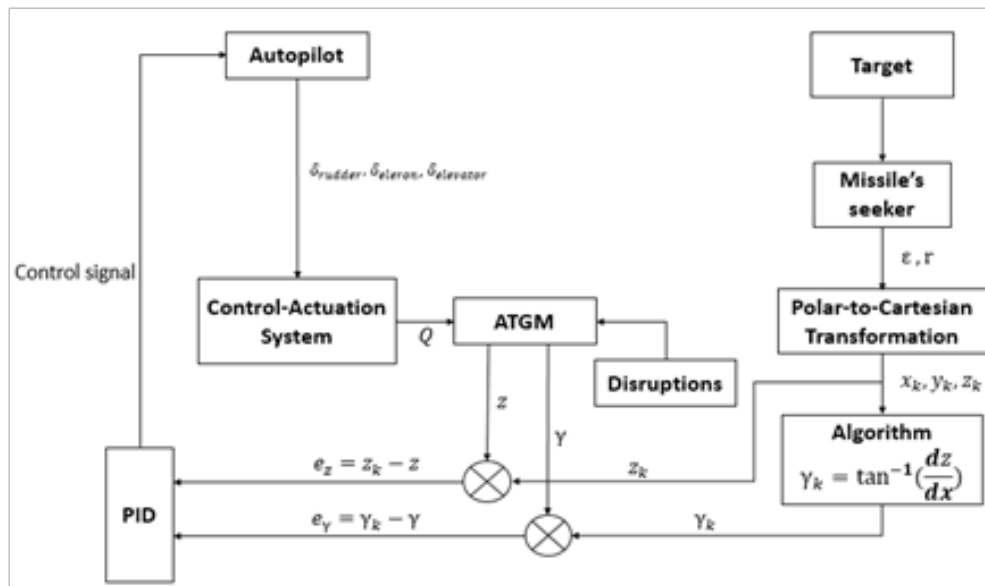


Fig. 4: Simplified diagram of ATGM control

By determining the error between the carried out path and the set one, the controlling forces are calculated in the autopilot. We assume that these forces in the simplest case can depend linearly on the error and its dynamic changes

(PID-Controller).

In the vertical plane<sup>[10]</sup>:

$$e_\gamma(t) = \gamma_k - \gamma \quad \text{and} \quad e_z(t) = z_k - z \quad (22)$$

$$Q_z = k_{\gamma p} e_\gamma + k_{\gamma i} \int e_\gamma dt + k_{\gamma d} \frac{de_\gamma}{dt} + k_{z p} e_z + k_{z i} \int e_z dt + k_{z d} \frac{de_z}{dt} \quad (23)$$

In the horizontal plane:

$$e_x(t) = x_k - x \quad \text{and} \quad e_y(t) = y_k - y \quad (24)$$

$$Q_y = k_{x p} e_x + k_{x i} \int e_x dt + k_{x d} \frac{de_x}{dt} + k_{y p} e_y + k_{y i} \int e_y dt + k_{y d} \frac{de_y}{dt} \quad (25)$$

Where  $(\gamma_k, \chi_k)$  are the desired flight path angles,  $(\gamma, \chi)$  is the actual current flight path angles,  $(z_k, y_k)$  are the desired points,  $(x, y, z)$  are the actual current missile's coordinates and  $(k_p, k_i, k_d)$  are the PID gains. PID parameters tuning has different methodologies to be defined, the dynamic model for controllers' parameters tuning techniques for frequency response and the classical PID controller design time response domains are studied to get regions of stability. PID controller design for both Single-Input-Single-Output (SISO) and Multi-Input-Multi-Output (MIMO) is presented in reference<sup>[12, 13]</sup>.

We already have the polynomial curve, which represents the flight altitude at a given moment time:

$$z_k = ax^3 + bx^2 + cx + d \quad (26)$$

$$\gamma_k = \tan^{-1}(3ax^2 + 2bx + c) \quad (27)$$

During the flight, many factors affected the missile's behavior in space. Starting with the aerodynamic forces, thrust, the Coriolis force, pushed the forces that disrupt its flight, such as normal winds for example. Considerations exclude climatic conditions, winds, and other external

interventions. Figure 4 provides a simplified diagram for ATGM control operation. The control is carried out by making use of the Q control force generated by the control system. The control signals are calculated by the proportional, integral, and differential (PID) controller. The controller argument is the deviation between the desired flight path angle and the actual one and the deviation between the desired flight altitude and the actual one:

$$e_\gamma(t) = \gamma_k - \gamma \quad \text{and} \quad e_z(t) = z_k - z \quad (28)$$

Where, the reference angle of control  $\gamma_k$  and reference flight altitude  $z_k$  are determined based on the polynomial function.

### III. THE EQUATIONS OF MOTION OF ATGM

Assuming that the missile is a rigid body that moves in the lower layers of the atmosphere (close to the earth's surface), the equations of its motion are as follows<sup>[14, 15]</sup>:

$$\frac{dV_m}{dt} = \frac{P}{m} \cos(\alpha) \cos(\beta) - g \sin(\gamma) \cos(\chi) - \lambda_x V_m^2 \quad (29)$$

$$\frac{d\gamma}{dt} = \frac{1}{V_m \cos(\chi)} \left( \frac{P}{m} \sin(\alpha) \cos(\beta) - g \cos(\gamma) + \lambda_z V_m^2 \alpha + \frac{Q_z + Z_k}{m} \right) \quad (30)$$

$$\frac{d\chi}{dt} = \frac{1}{V_m} \left( \frac{P}{m} \sin(\beta) + g \cos(\gamma) \sin(\chi) - \lambda_y V_m^2 \beta - \frac{Q_y + Y_k}{m} \right) \quad (31)$$

$$\ddot{\vartheta} \cos(\psi) - \dot{\vartheta} \dot{\psi} \sin(\psi) + \left( \frac{J_{ok}}{J_k} - 1 \right) \dot{\psi} \dot{\vartheta} \sin(\psi) = -D_1 \frac{V^2}{I} \alpha - D_2 V \dot{\alpha} - D_3 V \dot{\vartheta} + \frac{MQ\zeta}{J_k} \quad (32)$$

$$\ddot{\psi} - \left( \frac{J_{ok}}{J_k} - 1 \right) \dot{\vartheta}^2 \sin(\psi) \cos(\psi) = -D_1 \frac{\beta}{L} V^2 - D_2 V \dot{\beta} - D_3 V \dot{\psi} + \frac{MQ\zeta}{J_k} \quad (33)$$

Whereas, the same equations in the function of  $(x)$  have the form

$$\frac{dV_m}{dx} = \frac{\sqrt{1 + (\dot{z}(x))^2}}{V_m} \left( \frac{P}{m} - g \dot{z}(x) - \lambda_x V_m^2 \right) \quad (34)$$

$$\frac{d\gamma}{dx} = \frac{\sqrt{1+(z(x))^2}}{V_m} \left[ \left( \frac{P}{mV_m} + \lambda_z V_m \right) (\vartheta - \gamma) - \frac{g}{V_m} \cos(\gamma) + \frac{Q_z + Z_k}{mV_m} \right] \quad (35)$$

$$\frac{d\chi}{dx} = \frac{\sqrt{1+(z(x))^2}}{V_m} \left[ \left( \frac{P}{mV_m} + \lambda_z V_m \right) (\psi - \chi) - \frac{g}{V_m} \chi \cos(\gamma) + \frac{Q_z + Z_k}{mV_m} \right] \quad (36)$$

$$\begin{aligned} \frac{d^2\vartheta}{dx^2} - \left( \frac{J_{ok}}{J_k} - 1 \right) \frac{V^2}{1-(z(x))^2} \left( \frac{d\vartheta}{dx} \right)^2 = & - \left( \frac{dV}{dx} - V \frac{z(x)z''(x)}{1+(z(x))^2} \right) \frac{d\vartheta}{dx} - \\ D_1 \frac{\alpha}{L} \left[ 1 + (z(x))^2 \right] + \frac{z''(x)}{\sqrt{1+(z(x))^2}} - (D_2 + D_3) \sqrt{1+(z(x))^2} \frac{d\vartheta}{dx} + & \frac{M_\zeta}{J_k} \frac{1}{V^2(\cos(\gamma))^2} \end{aligned} \quad (37)$$

$$\begin{aligned} \frac{d^2\psi}{dx^2} = & - \left( \frac{dV}{dx} - V \frac{z(x)z''(x)}{1+(z(x))^2} \right) \frac{d\psi}{dx} - D_1 \frac{\beta}{L} \left[ 1 + (z(x))^2 \right] + \\ D_2 \sqrt{1+(z(x))^2} \frac{d\chi}{dx} - (D_2 + D_3) \sqrt{1+(z(x))^2} \frac{d\psi}{dx} + & \frac{M_\eta}{J_k} \frac{1}{V^2(\cos(\gamma))^2} \end{aligned} \quad (38)$$

Where,

$$\alpha = \vartheta - \gamma \quad \text{and} \quad \beta = \psi - \chi \quad (39)$$

$$D_1 = \frac{c_{lL}}{J_k}, D_2 = \frac{c_{nL}}{J_k}, D_3 = \frac{c_{mL}}{J_k} \quad (40)$$

$$\lambda_x = c_x \frac{\rho S}{2m}, \lambda_y = c_y \frac{\rho S}{2m}, \lambda_z = c_z \frac{\rho S}{2m} \quad (41)$$

#### IV. SIMULATION AND RESULTS

Investigations have been carried out via a 6-DOF model of an ATGM, using MATLAB/Simulink. Various scenarios of interception have been investigated in Table 1 (a long-range scenario with LOBL mode, a long-range scenario with LOAL mode). For long-range scenarios, the launching angle was fixed at 18° and the impact

angle was assumed to be -45° (the impact angle could be increased or decreased, but that angle was adopted because it's appropriate to achieve the maximum effectiveness of the warhead). From Table 1, it's obvious that in an interception scenario with a moving target, the desired impact angle is deviated around the desired final flight path angle according to the relation in (20). Extensive analysis has been carried out for each scenario, obtaining (missile trajectory, flight-path angle profile, executed flight path angle error profile, missile angle of attack). It's clear from analysis of each scenario that the angle of attack didn't exceed 5° (except for the launch-phase), which means achieving a small drag force on the missile's body while executing its pre-designed trajectory. It's also clear that the error (for flight path angle) during the launch-phase are of relatively large values due to several reasons, the most important of which is the transition phase between booster shut-off and sustainer ignition.

A. Simulation results for long-range ATGM with LOBL mode (stationary target at a range of 4000 m).

As shown in Figure 5, the missile trajectory follows the polynomial curve and intercept the target from the upper ceiling with sufficient kill probability as the miss distance is about (0.1 m). In Figure 6 and Figure 7, the efficiency of the proposed controller is obvious as it rapidly compensates the error between the desired and actual flight path angles. The final flight path angle  $\gamma_{mf}$  is achieved to be equals the desired impact angle  $\epsilon_{imp}$  (according to the relationship in equation (20) ), as the target is stationary. In Figure 8, it's obvious that the missile's angle of attack didn't exceed  $5^\circ$  (except for the launch-phase), which means achieving a small drag force on the missile's body while executing its predesigned trajectory.

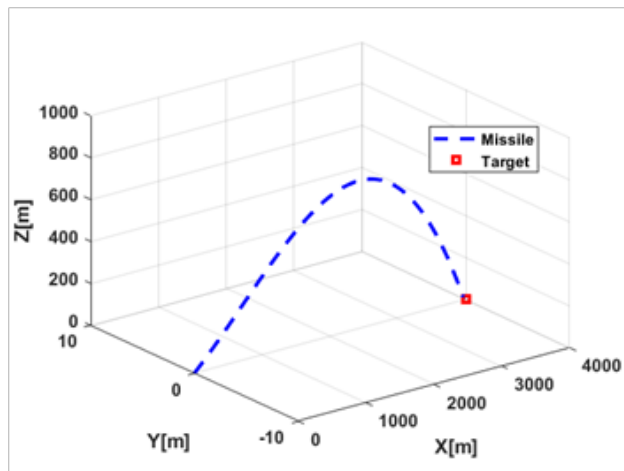


Fig. 5: Missile/Target Interception Scenario for a Stationary Target at 4000 m

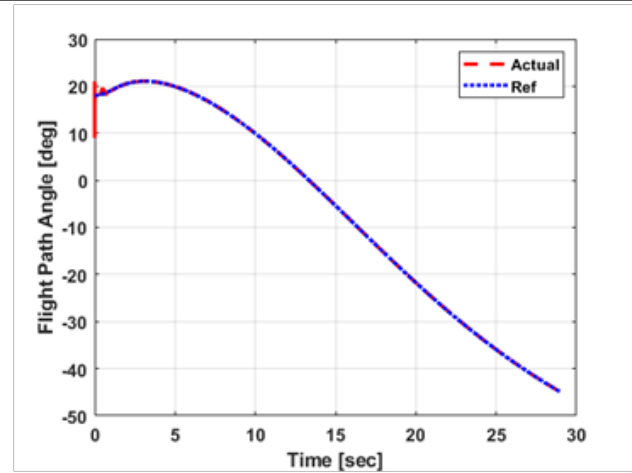


Fig. 6: Actual Flight Path Angle vs Reference

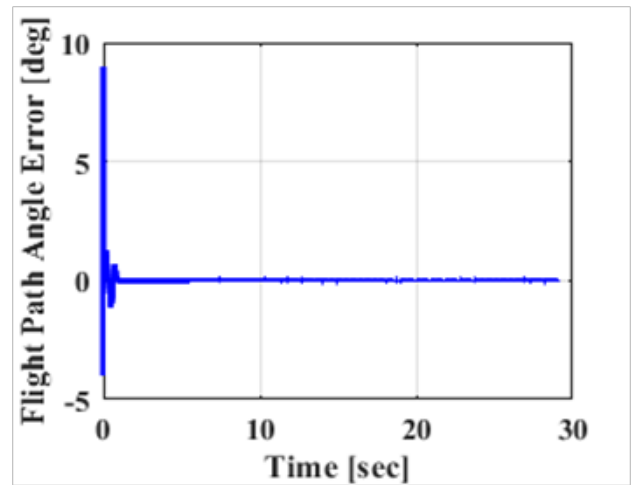


Fig. 7: Flight Path Angle Error Profile

Table 1: Simulation Results for various Scenarios

	Scenario	Miss Distance (m)	Launch Angle ( $^\circ$ )	Desired Final Flight Path Angle ( $^\circ$ )	Desired Impact Angle ( $^\circ$ )	Executed Impact Angle ( $^\circ$ )
LOBL	Stationary target at 4000 m	0.1	18	-45	-45	-44.98
	Moving (approaching) target (40 km/h) at 4000 m	0.399	18	-42.42	-45	-44.84
	Stationary target at 3250 m	0.16	18	-45	-45	-45.40
	Moving (approaching) target (40 km/h) at 3250 m	0.28	18	-42.26	-45	-44.48
	Stationary target at 2500 m	0.67	18	-45	-45	-44.96
	Moving (approaching) target (40 km/h) at 2500 m	0.178	18	-42.55	-45	-44.40
LOAL	Stationary target at 4000 m	0.1	18	-45	-45	-44.98
	Moving (approaching) target (40 km/h) at 4000 m	0.384	18	-42.42	-45	-45.24
	Stationary target at 3250 m	0.3	18	-45	-45	-45.03
	Moving (approaching) target (40 km/h) at 3250 m	0.262	18	-42.26	-45	-44.68
	Stationary target at 2500 m	0.694	18	-45	-45	-46.95
	Moving (approaching) target (40 km/h) at 2500 m	0.157	18	-42.55	-45	-44.64

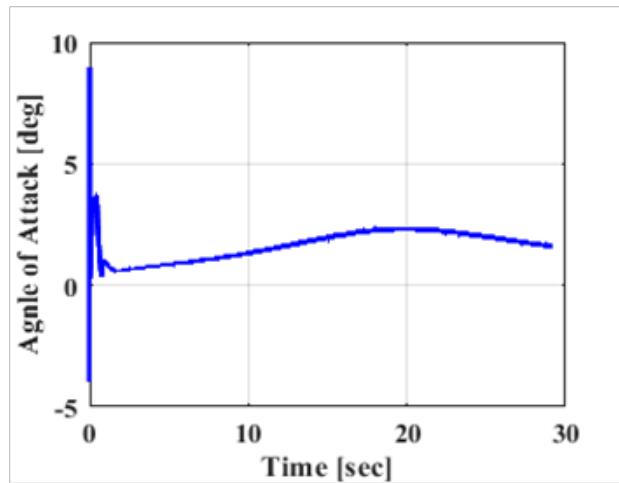


Fig. 8: Angle of Attack Profile

B. Simulation results for long-range ATGM with LOBL mode (moving target at a range of 4000 m).

In Figure 9, the missile trajectory follows the polynomial curve and intercept the target from the upper ceiling with sufficient kill probability as the miss distance is about (0.399 m). In Figure 10 and Figure 11, The deviation between the desired and actual flight path angles is due to the relation in equation (20) to achieve the desired impact angle of  $-45^\circ$  where the tuned desired final flight path angle  $\gamma_{mf}$  of  $-42.42^\circ$ , provides an actual flight path angle equals  $-44.84^\circ$  (the desired impact angle  $\epsilon_{imp}$  equals  $-45^\circ$ ). In Figure 12, it's obvious that the missile's angle of attack didn't exceed  $5^\circ$  (except for the launch-phase), which means achieving a small drag force on the missile's body while executing its predesigned trajectory.

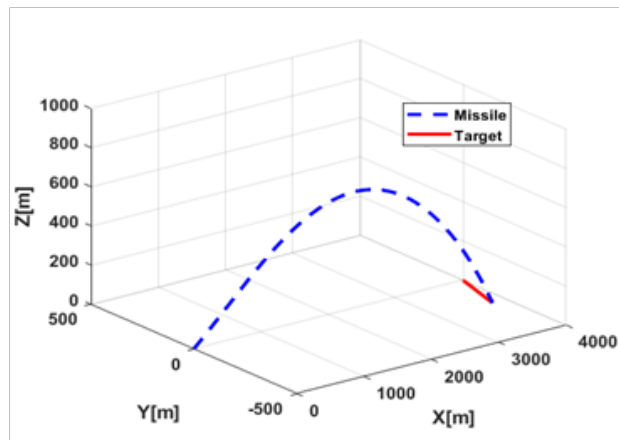


Fig. 9: Missile/Target Interception Scenario for a Moving Target at 4000 m

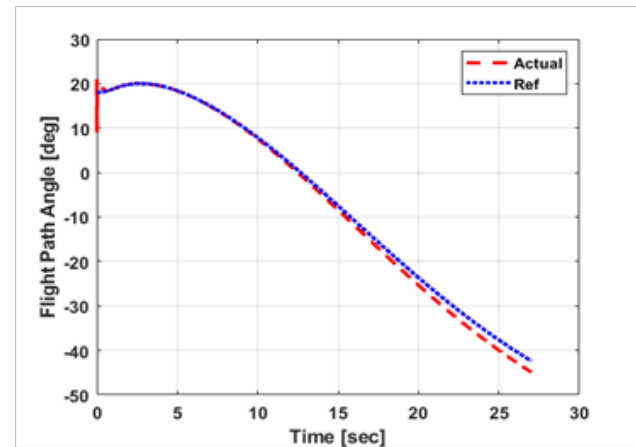


Fig. 10: Actual Flight Path Angle vs Reference

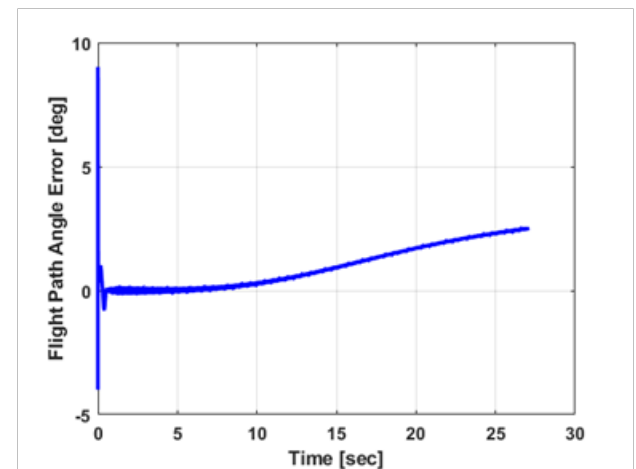


Fig. 11: Flight Path Angle Error Profile

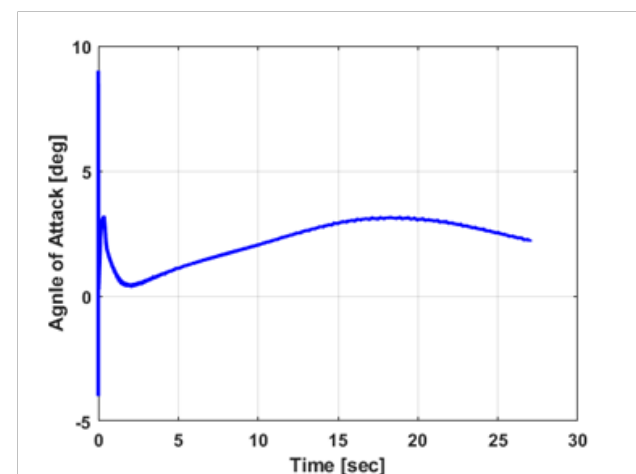


Fig. 12: Angle of Attack Profile

C. Simulation results for long-range ATGM with LOAL mode (stationary target at a range of 4000 m).

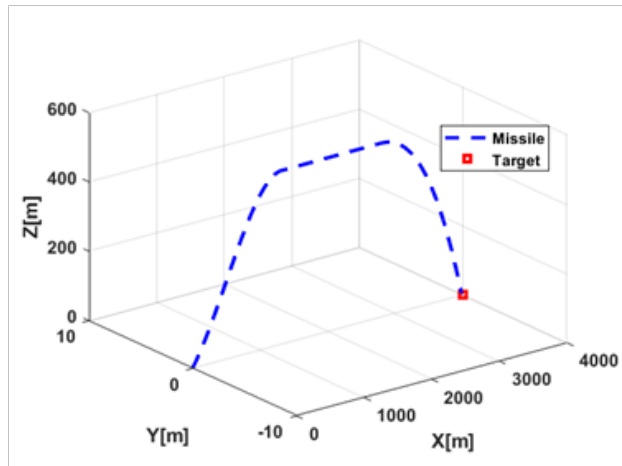


Fig. 13: Missile/Target Interception Scenario for a Stationary Target at 4000 m

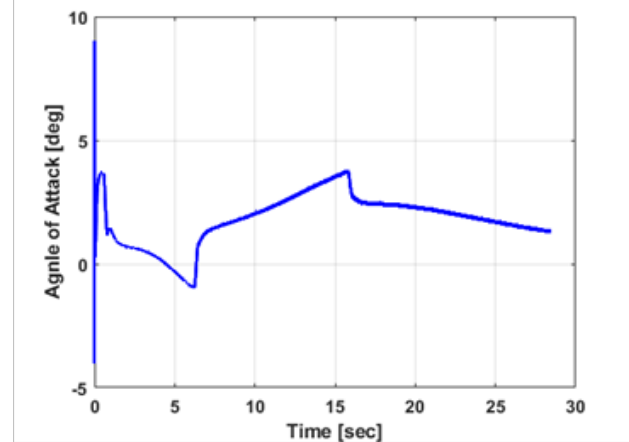


Fig. 16: Angle of Attack Profile

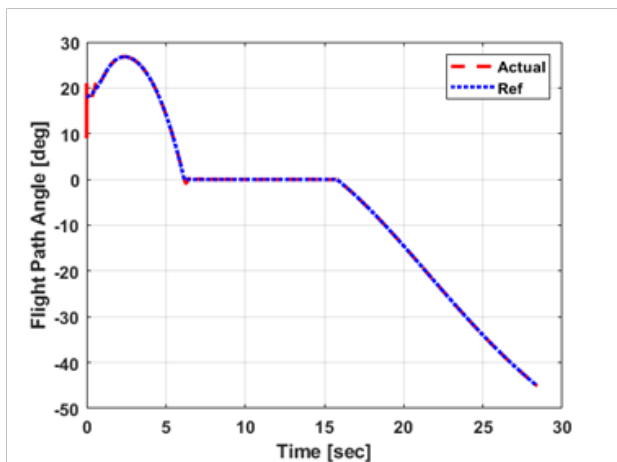


Fig. 14: Actual Flight Path Angle vs Reference

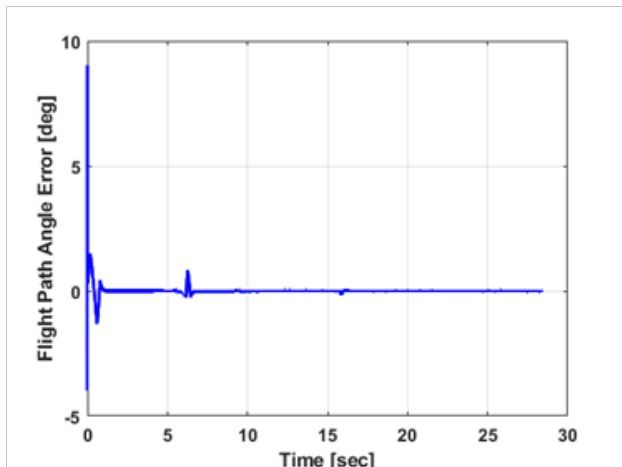


Fig. 15: Flight Path Angle Error Profile

As shown in Figure 13, the missile trajectory follows the polynomial curves, as the trajectory is divided into 3 stages (launch stage, med-coarse stage, interception stage). The missile intercepts the target from the upper ceiling with sufficient kill probability as the miss distance is about (0.1 m).

In Figure 14&Figure 15, the efficiency of the proposed controller is obvious as it rapidly compensates the error between the desired and actual flight path angles. The final flight path angle  $\gamma_{mf}$  is achieved to be equals the desired impact angle  $\epsilon_{imp}$  (according to the relationship in equation (20) ), as the target is stationary. In Figure 16, it's obvious that the missile's angle of attack didn't exceed  $5^\circ$  (except for the launch-phase), which means achieving a small drag force on the missile's body while executing its predesigned trajectory.

D. Simulation results for long-range ATGM with LOAL mode (stationary target at a range of 4000 m).

In Figure 17, the missile trajectory follows the polynomial curves, as the trajectory is divided into 3 stages (launch stage, med-coarse stage, interception stage). The missile intercepts the target from the upper ceiling with sufficient kill probability as the miss distance is about (0.384 m). In Figure 18&Figure 19, The deviation between the desired an actual flight path angles is due to the relation in equation (20) to achieve the desired impact angle of  $-45^\circ$  where the tuned desired final flight path angle  $\gamma_{mf}$  of  $-42.42^\circ$ , provides an actual flight path angle equals  $-45.24^\circ$  (the desired impact angle  $\epsilon_{imp}$  equals  $-45^\circ$ ). In Figure 20 it's obvious that the missile's angle of attack didn't exceed  $5^\circ$  (except for the launch-phase), which means achieving a small drag force on the missile's body while executing its predesigned trajectory.

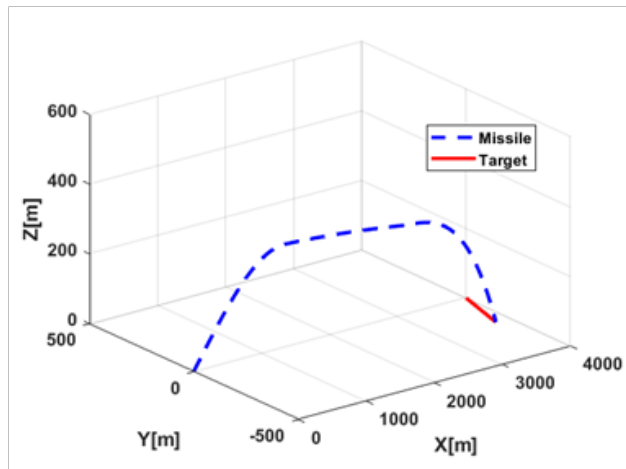


Fig. 17: Missile/Target Interception Scenario for a Moving Target at 4000 m

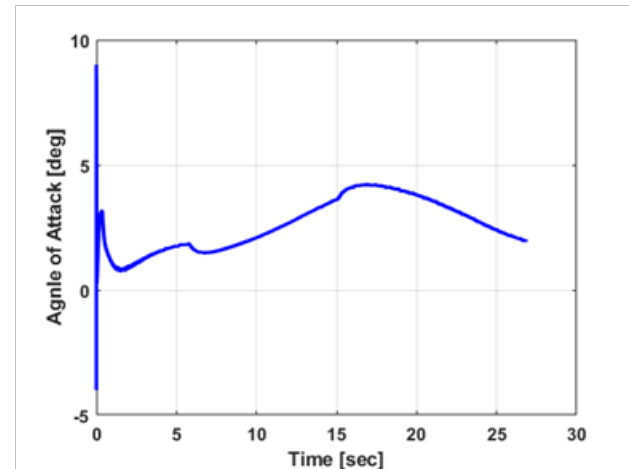


Fig. 20: Trajectory Error Profile (Elevation-Plane)

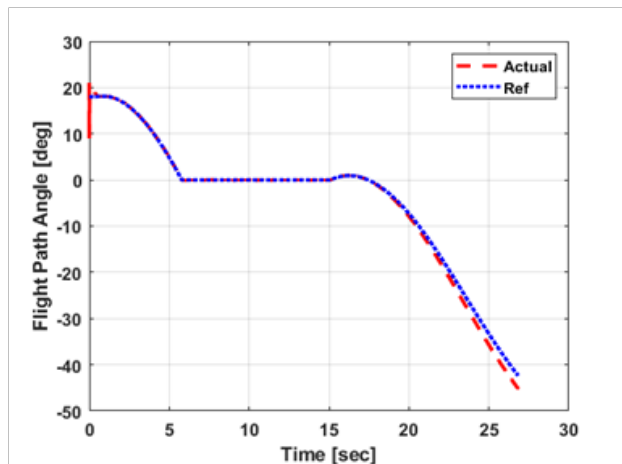


Fig.18: Actual Flight Path Angle vs Reference

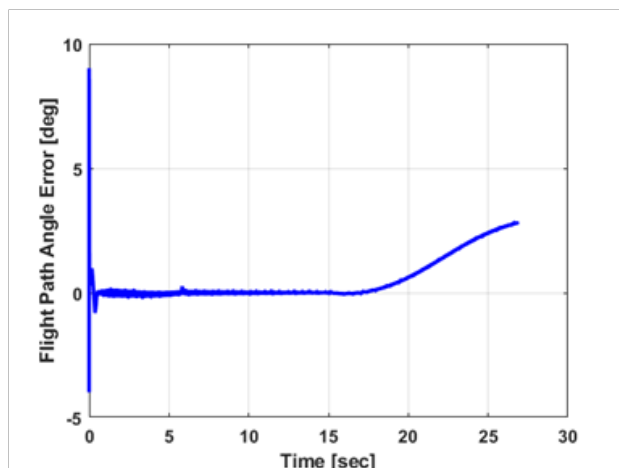


Fig. 19: Flight Path Angle Error Profile

## V. CONCLUSION AND FUTURE WORK

In this paper, a top-attack missile guidance law based on polynomial function and impact angle constraints is proposed to achieve a high kill probability for different types of targets. The proposed algorithm calculates the appropriate impact angle to achieve the maximum penetration of tanks' armors. The guidance algorithm is evaluated via 6-DOF simulation using the Matlab/Simulink platform. The simulation model includes sub-models for navigation, guidance, control, autopilot, and airframe. The final miss distance is sufficient (around 1 m) considering the angle of attack limitations no to exceed 50 for minimizing the drag force during flight. In the presented scenarios (for long-range), the impact angle of -45 is adopted.

The contribution of this work can be summarized as follows:

The polynomial guidance law introduced in previous publications is modified for applying impact angle constraints (as shown in equation No (20, 21)) in the descending phase for increasing the kill probability of the anti-tank missiles comparing with previous publications.

The modified guidance law is adopted to deal with the moving targets.

The missile control is relatively turbulent in the transient phase between booster shut-off and sustainer motor ignition but this will be taken into account and addressed later. This work can be extended by applying frequency domain analysis to evaluate the proposed algorithm frequency domain stability parameters (gain margin and phase margin), and then design a suitable controller in frequency domain. Further, implementing this program on microprocessors and running processor-in-loop simulation (PIL) and hardware-in-loop simulation (HIL) to evaluate

the routing software performance.

## VI. NOMENCLATURE

### IIR IMAGING INFRA-RED

CCD CHARGED-COUPLED DEVICE

$C_m, C_n, C_l$  AERODYNAMIC MOMENT COEFFICIENTS

$C_x, C_y, C_z$  AERODYNAMIC FORCE COEFFICIENTS

$g$  Gravitational acceleration

$J_{ok}, J_k$  Missile moment of inertia concerning the horizontal and vertical axis

$L, m$  Missile's length and Mass

$M_x, M_y$  The external moment about the center of mass

$P$  Total thrust

$Q$  Controlling force

$Q_y, Q_z$  External controlling forces

$S$  Missile's reference area

$V_m, a_m$  Missile velocity and acceleration vectors

$X, Y, Z$  Cartesian Coordinates

$\alpha, \beta$  Missile angle of attack and sideslip angle

$\gamma, \chi$  Flight-path angle in the vertical plane and horizontal plane

$\varepsilon$  Line of sight angle (LOS)

$\vartheta, \psi$  Pitch and Yaw angle

$\lambda_x, \lambda_y, \lambda_z$  Coefficients of aerodynamic forces

$\rho$  Air density

## VII. REFERENCES

- [1] H. B. Oza and R. Padhi, "Impact-angle-constrained suboptimal model predictive static programming guidance of air-to-ground missiles," *J. Guid. Control. Dyn.*, vol. 35, no. 1, pp. 153–164, 2012, doi: 10.2514/1.53647.
- [2] B. G. Park, T. H. Kim, and M. J. Tahk, "Optimal impact angle control

guidance law considering the seeker's field-of-view limits," *Proc. Inst. Mech. Eng. Part G J. Aerosp. Eng.*, vol. 227, no. 8, pp. 1347–1364, 2013, doi: 10.1177/0954410012452367.

[3] N. R. Iyer, "Recent Advances in Antitank Guided Missile Systems .," *Def. Sci. J.*, vol. 45, no. 3, pp. 187–197, 1995, doi: 10.14429/dsj.45.4118.

[4] J. Harris and N. Slegers, "Performance of a fire-and-forget anti-tank missile with a damaged wing," *Math. Comput. Model.*, vol. 50, no. 1–2, pp. 292–305, 2009, doi: 10.1016/j.mcm.2009.02.009.

[5] E. H. Kapeel, M. A. H. Abozied, A. M. Kamel, and H. Hendy, "Evaluation of Missile Terminal Guidance Using Software in Loop (SIL)," 2020 12th Int. Conf. Electr. Eng. ICEENG 2020, pp. 389–395, 2020, doi: 10.1109/ICEENG45378.2020.9171703.

[6] E. Kim, H. Cho, and Y. Lee, "Terminal guidance algorithms of missiles maneuvering in the vertical plane," 1996 *Guid. Navig. Control Conf. Exhib.*, no. July, pp. 1–7, 1996, doi: 10.2514/6.1996-3883.

[7] C. V. Sirisha and R. Das, "Guidance philosophy for impact angle maximization for anti-tank flight vehicle," *IFAC-PapersOnLine*, vol. 49, no. 1, pp. 12–17, 2016, doi: 10.1016/j.ifacol.2016.03.021.

[8] He, S., Lee, C.H., Shin, H.S. and Tsourdos, A., 2020. *Optimal Guidance and Its Applications in Missiles and UAVs*. Springer Nature.

[9] X. Wang and X. Lu, "Three-dimensional impact angle constrained distributed guidance law design for cooperative attacks," *ISA Trans.*, vol. 73, pp. 79–90, 2018, doi: 10.1016/j.isatra.2017.12.009.

[10] Z. Koruba and Ł. Nocoń, "Automatic control of an anti-tank guided missile based on polynomial functions," *J. Theor. Appl. Mech.*, vol. 53, no. 1, pp. 139–150, 2015, doi: 10.15632/jtam-pl.53.1.139.

[11] L. Sun, W. Wang, R. Yi, and S. Xiong, "A novel guidance law using fast terminal sliding mode control with impact angle constraints," *ISA Trans.*, vol. 64, pp. 12–23, 2016, doi: 10.1016/j.isatra.2016.05.004.

[12] H. Hendy, X. T. Rui, Q. B. Zhou, F. F. Yang, and M. Khalil, "Transfer matrix method for multibody systems of TITO system control applications," *Appl. Mech. Mater.*, vol. 530–531, pp. 1043–1048, 2014, doi: 10.4028/www.scientific.net/AMM.530-531.1043.

[13] H. Hendy, X. Rui, Q. Zhou, and M. Khalil, "Controller parameters tuning based on transfer matrix method for multibody systems," *Adv. Mech. Eng.*, vol. 2014, 2014, doi: 10.1155/2014/957684.

[14] M. Khalil, X. Rui, Q. Zha, H. Yu, and H. Hendy, "Projectile impact point prediction based on self-propelled artillery dynamics and doppler radar measurements," *Adv. Mech. Eng.*, vol. 2013, 2013, doi: 10.1155/2013/153913.

[15] Islam H. Elandy, "Modeling and Simulation of an Aerial Gliding Body in Free-Fall," *Int. J. Eng. Res.*, vol. V7, no. 08, pp. 3–11, 2018, doi: 10.17577/ijertv7is080046.